Available online at www.sciencedirect.com
ScienceDirect
Journal of Power Sources 162 (2006) 1010–1022
JOURNAL OF POWER SOURCES
www.elsevier.com/locate/jpowsour

Electrochemical impedance spectroscopy study of methanol oxidation on nanoparticulate PtRu direct methanol fuel cell anodes: Kinetics and performance evaluation

Debasish Chakraborty [a,b], Ib Chorkendorff [a,c], Tue Johannessen [b,*]

[a] *Center for Individual Nanoparticle Functionality (CINF), Technical University of Denmark, Dk-2800 Kgs. Lyngby, Denmark*
[b] *Aerosol Laboratory, Nano DTU, Department of Chemical Engineering, Technical University of Denmark, Dk-2800 Kgs. Lyngby, Denmark*
[c] *Department of Physics, Technical University of Denmark, Dk-2800 Kgs. Lyngby, Denmark*

Received 10 March 2006; received in revised form 3 August 2006; accepted 3 August 2006
Available online 20 September 2006

Abstract

Electrochemical impedance spectroscopy (EIS) along with cyclic voltammetry (CV) has been applied as a tool for the mechanistic investigation of methanol oxidation on nanoparticulate PtRu fuel cell anodes of a commercially available state of the art membrane electrode assembly (MEA). The spectra could be fitted to a circuit derived analytically for multi-step single adsorbed intermediate reactions. The analysis has indicated that methanol adsorption and surface blocking occur below the onset and the surface is 'poisoned' to the highest degree just before the onset, implying that the removal of residues before the onset, if any, is slower compared to the formation. The onset potential is marked by a sudden change in the mechanism as the impedance becomes pseudoinductive. It has also been demonstrated that EIS can be applied for analyzing and singling out different contributions behind electrode performance for methanol oxidation reaction under fuel cell operating condition.

Keywords: Electrooxidation; DMFC; Pseudoinductive behavior; Double layer capacitance; Electroactive surface area; Membrane conductivity

1. Introduction

Depletion of petroleum reserves, global warming and the concern about energy security have inspired the search for new energy carriers other than petroleum. Methanol is an excellent energy carrier because it is liquid at room temperature and pressure and can be produced from diverse sources including natural gas, coal and biomass. The fact that methanol is liquid makes it especially attractive as an energy carrier in mobile applications. Unlike hydrogen, storage of methanol is not problematic and if methanol is used as fuel, the existing fuel infrastructure could be utilized without much modification. Although, using methanol as fuel in road transportation will not eliminate the emission of CO_2 to the atmosphere, the inherent higher efficiency of fuel cells compared to internal combustion engines could substantially lower the emission of CO_2 [1]. In direct methanol fuel cells (DMFC), methanol can be fed directly for the purpose of converting chemical energy to electrical energy. Besides transportation applications, DMFC is getting more and more attention as a replacement for secondary batteries. DMFCs have near term market penetration potential in this area with transport being the longer term goal [2]. However, to use methanol in fuel cells commercially, some serious technological challenges like the sluggish kinetics of methanol oxidation reaction and the crossover of methanol to the cathode must be overcome.

The complete anodic oxidation of methanol is described by:

$$CH_3OH + H_2O \rightarrow CO_2 + 6H^+ + 6e^- \quad (1)$$

Thermodynamically, this reaction has quite low equilibrium potential (0.016 V versus standard hydrogen electrode, SHE at 25 °C) [3]. But the oxidation of methanol requires a large overpotential, i.e. 0.2–0.4 V depending on the catalyst and operating conditions [4]. The complete oxidation of methanol requires the transfer of six electrons, resulting in sluggish kinetics even on PtRu, the widely accepted best catalyst available for the reaction. Therefore, it is important to investigate the mechanism of

* Corresponding author. Tel.: +45 45252924; fax: +45 45882258.
E-mail address: tj@kt.dtu.dk (T. Johannessen).

0378-7753/$ – see front matter © 2006 Elsevier B.V. All rights reserved.
doi:10.1016/j.jpowsour.2006.08.010

Table 1
Specification of four different MEAs used in the work

MEA	Anode	Cathode	GDL	Membrane	Applied temperature and duration
IRD	PtRu (1:1) (Johnson Matthey); ∼2 mg cm^{-2}	∼56% Pt/C (Johnson Matthey)	Toray TGPH090	Nafion 117	∼140 °C; 5 min
JM	PtRu (1:1) (Johnson Matthey); ∼1.5 mg cm^{-2}	∼20%Pt/C (E-TEK); 2 mg cm^{-2}	Toray TGPH090	Nafion 117	∼130 °C; 5 min
Flame	PtRu (1:1); ∼1.5 mg cm^{-2}	∼20%Pt/C (E-TEK); 2 mg cm^{-2}	Toray TGPH090	Nafion 112	∼140 °C; 5 min

this reaction on PtRu for increasing the noble metal utilization as well as designing novel catalysts for the reaction.

It is well known that methanol electrooxidation involves several reaction steps with different rates; electrochemical impedance spectroscopy (EIS) can distinguish processes with different time constants, and with this method it might be possible to distinguish different elementary steps of the reaction [5,6]. Although several studies have used EIS to investigate methanol electrooxidation [7–16], to our knowledge only three reports have focused on the mechanistic aspects of methanol oxidation in a DMFC using nanoparticulate catalysts [7,8,16]. Impedance analysis of methanol oxidation in a 'real world electrode environment' is important not only to have a clearer understanding of the reaction at the three-phase region, but also to avoid artifacts arising from anion adsorption which results from electrolytes like H_2SO_4 which contains mobile anions [17]. Jiang and Kucernak have reported that the discharge of methanol on Pt is shifted to more negative potentials when Nafion is used as electrolyte instead of H_2SO_4. They attributed the phenomenon to the absence of mobile anions in Nafion [18]. Moreover, it has also been reported that Nafion coating greatly enhances the methanol oxidation activity on Pt [19]. For the analysis of methanol electrooxidation reaction in this work, we used a single cell fuel cell setup with DMFC membrane electrode assembly (MEA) consisting of a nonoparticulate PtRu anode. Besides the mechanistic aspects, using impedance analysis on an MEA could produce important information on protonic conductivity of the catalyst layers [20], and membrane [21]; dependence of the membrane resistance on humidity and temperature [22]; thickness of the catalyst layer [23], etc. We have performed a detailed analysis of the methanol oxidation at the PtRu nanoparticulate anode of a state of the art commercial DMFC MEA both below and above the onset potentials. The impedance data along with the voltammetric measurements were used to obtain an in-depth mechanistic understanding. Finally, the findings were applied for investigating and comparing methanol oxidation performance of different in-house prepared MEAs to the commercial one.

2. Experimental

The electrochemical measurements were performed in a single cell test fuel cell described elsewhere [13]. Three different MEAs were used in this work. One type of MEA was the state of the art product obtained courtesy of IRD Fuel Cells A/S. This MEA, referred to as IRD for the rest of the article, was used for the detailed mechanistic investigation of methanol oxidation and establishing a basis for performance comparison between different MEAs. The second MEA, named as JM for the purpose of this article, was fabricated in-house by using an unsupported Johnson Matthey PtRu catalyst (1:1 atomic ratio, 1.5 mg cm^{-2}) as the anode. The cathode was a 20% Pt/C (E-TEK) painted on gas diffusion layer (GDL). The third MEA, named Flame, consisted of an anode synthesized by Flame pyrolysis with a loading of 1.5 mg cm^{-2} PtRu (1:1 atomic ratio). The fabrication of the Flame MEA has been discussed in detail in our previous article [13]. The geometric surface areas of the electrodes for all the three MEAs were 3.14 cm^2 and currents were normalized with the geometric area unless otherwise mentioned. Table 1 summarizes the specifications of the three different MEAs used. The anode of the fuel cell was fed with methanol solutions of different concentrations at a flow rate of 1 ml min^{-1}. The cathode, which also acted as a dynamic hydrogen electrode (DHE), was fed with H_2 [13,17,24]. All the potentials reported in this paper are given relative to a DHE. Two electrode impedance measurements of methanol oxidation in a fuel cell anode have been reported first by Müller et al. [8,25]. The reaction at the dynamic hydrogen electrode is as follows:

$$2H^+ + 2e \Leftrightarrow H_2 \quad (2)$$

In fuel cell research, this reaction is considered very fast compared to reactions like methanol oxidation or O_2 reduction. Because of this the impedance of the DHE can be considered negligible compared to the impedance of the anode side where methanol electrooxidation is occurring. The total impedance of the cell which is the sum of the anode impedance and the cathode impedance can be taken as the impedance of the anode side alone. In fact this assumption has been confirmed experimentally by Diard et al. [16]. The impedance measurements were taken from 100 kHz to 10.5 mHz by applying a sine wave of rms of 10 mV on top of the bias potentials with the potentiostat Parstat 2273 (Princeton Applied Research). The spectra were obtained in two different ways. For the mechanistic investigation, where it was necessary to obtain a huge number of spectra, single sine (100 kHz to 1 Hz) followed by a multi-sine (1.03 Hz to 10.5 mHz) technique was used. Using multi-sine techniques for obtaining low frequency data makes the process significantly faster. Melnick and Palmore [14,15] have also used the combination of single and multi-sine techniques to obtain impedance data for methanol oxidation on Pt. The single sine method for the whole range was used when spectra were measured for the purpose of performance comparisons between different MEAs. During impedance measurements, the perturbation was applied after taking the electrode to the bias potential and waiting for 1 min to establish a pseudo-steady

state. In between two different impedance measurements, the electrode potential was cycled five times from open circuit to 0.8 V at a scan rate of 50 mV s^{-1}. Before starting the real experiment, it was confirmed that the MEA was properly humidified and stable by flowing 1.0 M methanol solution at the anode and humidified hydrogen at the cathode for ∼4 h and taking occasional impedance spectra and cyclic voltammograms (CV). It was observed that the system was stable after ∼2 h.

Cyclic voltammograms were taken form open circuit potential to 0.8 V. For the stripping experiment, the anode was kept at open circuit potential for 6 min as the methanol flow started. This is the estimated time for methanol solution to travel from the reservoir to the cell outlet at 1 ml min^{-1}. The potential was then raised to 0.1 V for methanol adsorption and after 5 min, the methanol flow was replaced with water in order to remove any unreacted methanol from the anode compartment while the potential was maintained at 0.1 V. After 30 min of flushing, the stripping was performed by cycling the electrode potential from 0.1 V to 0.8 V at a scan rate of 5 mV s^{-1}.

Unless otherwise specified, all bias potentials and overpotentials have been corrected for iR losses in the cell by using the current from respective CVs and the membrane resistance, R_e, from impedance data fitting (see Section 4 for further details).

3. Results

Fig. 1 shows impedance behavior of room temperature (28 °C) methanol oxidation on nanoparticulate PtRu at various concentrations (0.1 M, 1.0 M and 10.0 M) and potentials. For all the concentrations reported in this paper, as the bias potential increases, the loops are inclined to bend towards the *x*-axes and at ∼0.32 V, intersect the *x*-axes. Fig. 1b and c shows the impedance behavior for a wider potential rage for 1.0 M methanol. The Nyquist plot (Fig. 1b) shows that the low frequency response

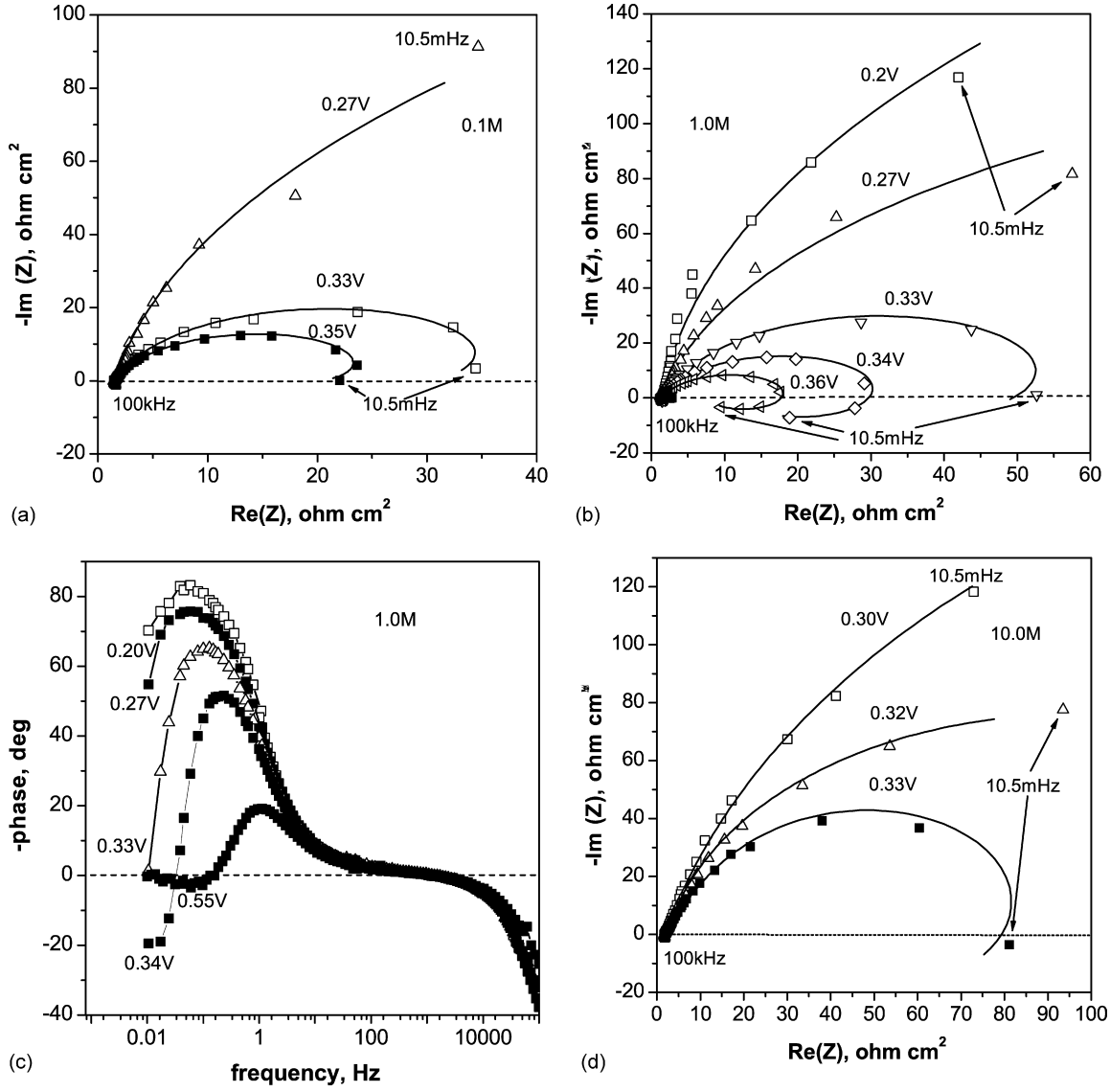

Fig. 1. Complex plane plot of impedance of 0.1 M (a), 1.0 M (b) and 10.0 M (d); also shown the Bode plot for 1.0 M methanol (c). Points: experimental; lines: fitted with equivalent circuit in Fig. 8a. Operating temperature: 28 °C; anode flow: 1 ml min^{-1}; cathode flow: H_2 at 5 ml min^{-1}. Bias potentials are corrected for iR losses in the cell.

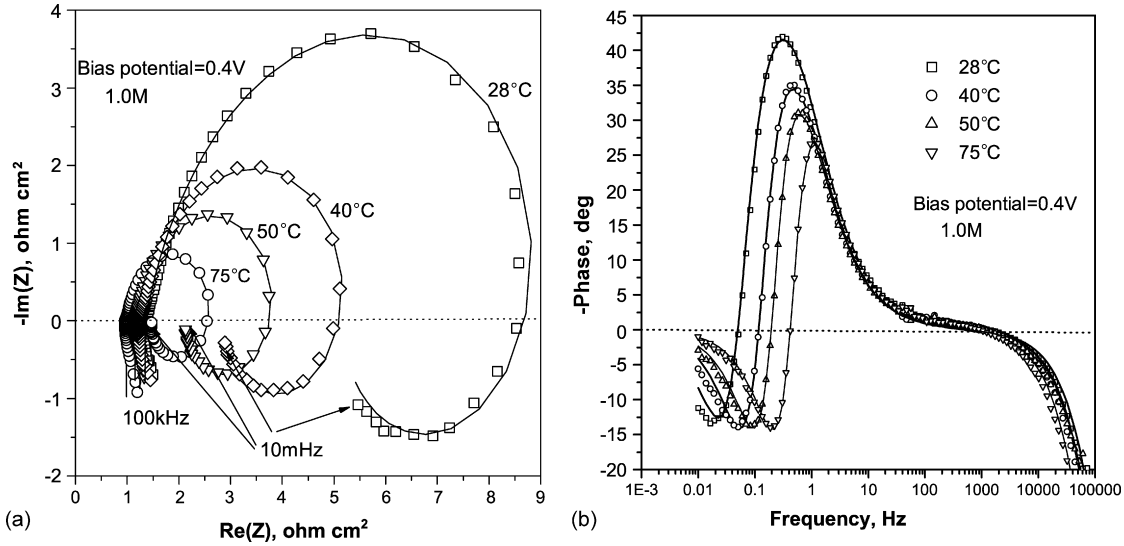

Fig. 2. Complex plane plot (a) and phase shift plot (b) of impedance for 1.0 M methanol at different temperatures at a bias potential of 0.4 V (uncorrected). Points: experimental; lines: fitted with equivalent circuit in Fig. 8a. Anode flow: 1 ml min^{-1}; cathode flow: H_2 at 5 ml min^{-1}.

becomes inductive as the potential is increased above 0.33 V. Also, as the potential increases, the "diameter" of both the capacitive and inductive loop decreases (even though these two are not perfect semicircles, diameter will be used here for ease of understanding). The appearance of the inductive behavior can also be observed from the phase shift (Bode) plot (Fig. 1c). At low bias potential (e.g. ~0.2 V), only one capacitive peak is visible. As the potential increases, the inductive peak appears like the inductive loop in the Nyquist plot. After 0.6 V (not shown), the low frequency inductive loop is no longer evident. However, another loop in the first quadrant appears which indicates that the reaction is limited by mass transfer. We shall not consider the mass transfer limited case in this paper. The temperature dependence of the impedance behavior at a constant bias potential (0.4 V, uncorrected) for 1.0 M methanol is shown in Fig. 2. The radius of both the capacitive and inductive loop (Fig. 2a) decrease as the temperature increases. The frequencies at which the capacitive and inductive peaks appear increase with temperature: e.g. from ~300 mHz and ~20 mHz, at 28 °C to ~1 Hz and ~200 mHz, respectively, at 75 °C (Fig. 2b). It has been observed that the appearance of the inductive loop occurs at lower potentials with increasing temperature (not shown).

Cyclic voltammetry plots for 0.1 M, 1.0 M and 10.0 M methanol solution at 28 °C (Fig. 3) reveal that the onset potential is around ~0.32 V and does not vary with concentration. Catalytic activity was clearly larger on 1.0 M methanol compared to 0.1 M methanol. However, little difference was observed between the 1.0 M and 10.0 M cases. The 0.1 M methanol solution shows serious transport limitation as observed by a very low limiting current of ~20 mA cm^{-2}. The current in the H_{UPD} (hydrogen underpotential deposition) region is dependent on concentration: the current densities at 0.1 V were ~4.5 mA cm^{-2}, ~8.6 mA cm^{-2} and 9.4 mA cm^{-2} for 10 M, 1 M and 0.1 M methanol solution, respectively. A blank CV done with only DI water at the anode is also shown in the figure.

An increase in temperature not only increases the activity of methanol oxidation, but also decreases the onset potential (Fig. 4). The onset potential for positive going scan for 1.0 M methanol decreases from ~0.32 V at 28 °C to ~0.2 V at 75 °C. The current in the H_{UPD} region is suppressed as the temperature is increased: at 0.15 V, the current densities are 9 mA cm^{-2}, 7.5 mA cm^{-2} and 5.3 mA cm^{-2} at 28 °C, 50 °C and 75 °C, respectively. This phenomenon could be attributed to the increased rate of methanol adsorption at elevated temperatures [18].

Fig. 5 shows the result of the residue stripping experiment with 0.1 M and 1.0 M methanol solution. The onset of the residue oxidation remained unchanged with bulk concentration of methanol at ~0.31 V. It can be seen from Fig. 5 that one

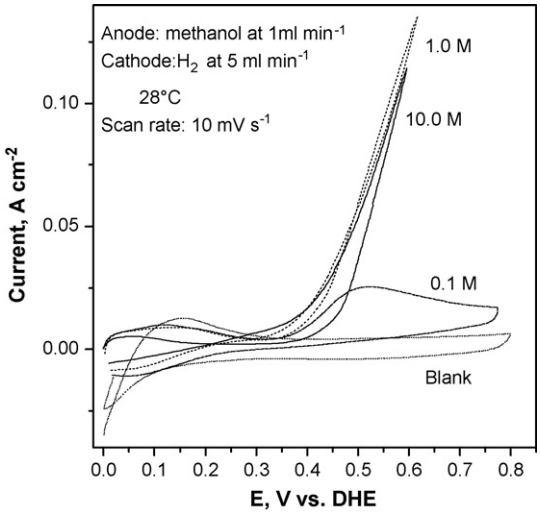

Fig. 3. CV plots for different concentration of methanol at 28 °C. A blank CV done by flowing only DI water through the anode chamber is also shown for comparison. Scan rate: 10 mV s^{-1}; anode flow: 1 ml min^{-1}; cathode flow: H_2 at 5 ml min^{-1}. Overpotentials are corrected for iR losses in the cell.

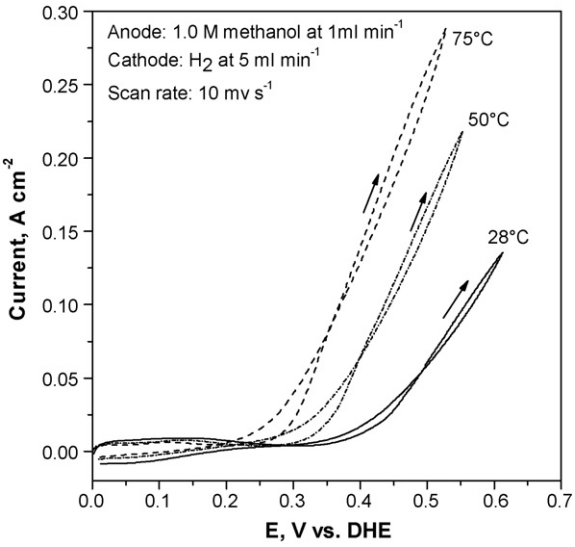

Fig. 4. CV plots for 1.0 M methanol at different temperatures. Scan rate: 10 mV s^{-1}; anode flow: 1 ml min^{-1}; cathode flow: H_2 at 5 ml min^{-1}. Overpotentials are corrected for iR losses in the cell.

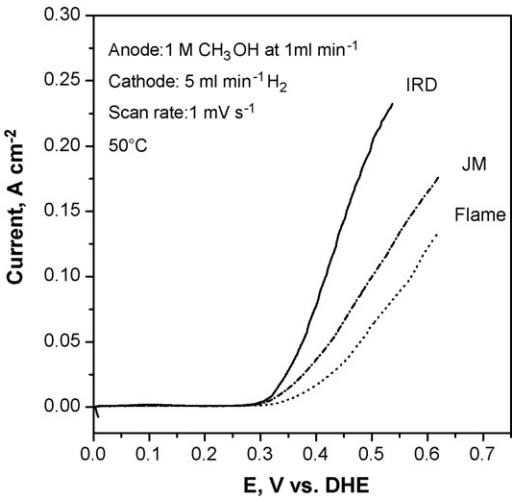

Fig. 6. Anode polarization curve for three different MEAs at 50 °C. Scan rate: 1 mV s^{-1}; anode flow: 1 ml min^{-1}; cathode flow: H_2 at 5 ml min^{-1}. Overpotentials are corrected for iR losses in the cell. The currents are normalized with geometric area of the electrodes.

complete cycle from 0.1 V to 0.8 V has not stripped all the residues from the surface. The total charge for stripping the residues formed form 0.1 M and 1.0 M methanol solution are 0.84 C cm^{-2} and 1.15 C cm^{-2}, respectively, indicating that the residue coverage is higher for higher concentrations of methanol. Similar results were obtained by Stimming and co-workers for methanol residue stripping experiment on PtRu/C [26]. It should be mentioned that the stripping charge has been normalized based on the geometrical surface area of the electrode and not the available three-phase boundary area. No splitting of the residue oxidation peak was observed indicating that the surface is homogenous in terms of Pt and Ru compositions [26].

Fig. 6 shows a comparison of the anode polarization curves of three different MEAs at 50 °C. It could be seen that the performance not only depends on the type of catalysts, but also on the preparation of the MEAs. The IRD MEA outperforms the rest tested for this work: the order being IRD > JM > Flame. At 0.4 V and 50 °C, the current densities are ~78 mA cm^{-2}, ~37 mA cm^{-2} and ~17 mA cm^{-2} for IRD, JM and Flame MEAs, respectively. The impedance responses have been shown in Fig. 7 at 0.4 V bias potentials at 50 °C. Each spectrum demonstrates a high frequency pseudocapacitive loop followed by a low frequency pseudoinductive loop with the diameters of the pseudocapacitive loops show a clear decreasing tendency in the order Flame > JM > IRD for 0.4 V.

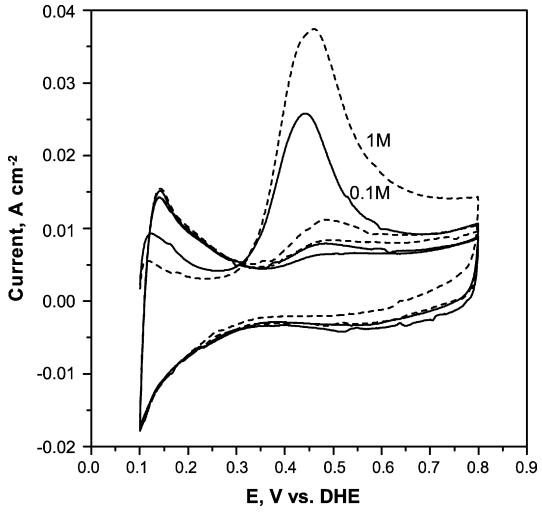

Fig. 5. CVs for adsorbate stripping at 5 mV s^{-1} after 5 min of the methanol adsorption from 1.0 M and 0.1 M solutions at 0.1 V. It could be observed that more than one cycle was necessary for complete oxidation. For easier understanding only first three cycles are shown. Both adsorption and stripping were done at 28 °C. Overpotentials are not corrected for iR losses in the cell.

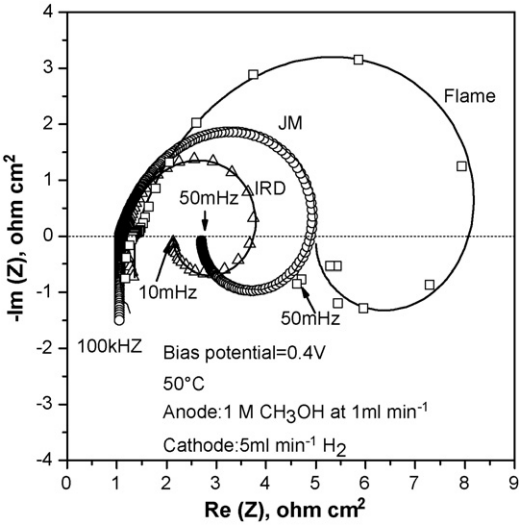

Fig. 7. Nyquist plot for different MEAs at a bias potential of 0.4 V. Points: experimental data; lines: fitted with equivalent circuit. Anode flow: 1 ml min^{-1}; cathode flow: H_2 at 5 ml min^{-1}; temperature: 50 °C.

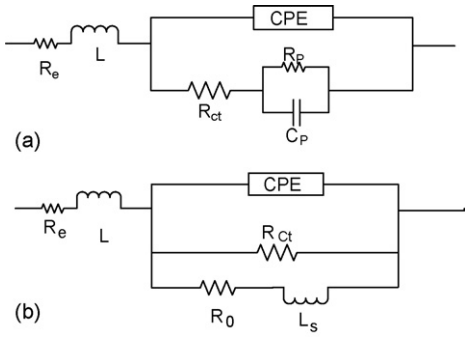

Fig. 8. Equivalent circuits used for fitting data (a) and a mathematical equivalent of the circuit (b). R_e: membrane resistance, L: high frequency inductance; R_{Ct}: charge transfer resistance; C_P: capacitance; R_P, R_0: resistances; L_s: low frequency inductance; CPE: constant phase element.

4. Equivalent circuit and modeling

The equivalent circuit which has been found suitable for fitting the impedance data is shown in Fig. 8a. This equivalent circuit typically represents impedance data for electrochemical reactions with single adsorbed intermediate where diffusion of participating species is not rate limiting. In the circuit, the capacitance C_P is related to the steady-state pseudocapacitance (described in more detail in Section 5). The resistance, R_P, in parallel to C_P, is associated with the adsorbate formation/removal [27,28]. The other resistance, R_{Ct}, is known as the charge transfer resistance and relates to the resistance of electron transfer to the electrode. In electrochemical cells, all Faradaic processes occur in parallel with a double layer charging so a double layer capacitance (C_{dl}) always comes into play whenever impedance measurements are done. Therefore, the double layer capacitor is connected parallel to the Faradaic branch of the circuit. However, possibly due to the dispersion of capacitance over the electrode surface area [6,29], a much improved fit of the data was obtained when the double layer ideal capacitor was replaced by a constant phase element (CPE), Y_0, whose impedance is defined by

$$Z_{CPE} = Y_0(j\omega)^{-n} \tag{3}$$

where n can have values between 0 and 1. When n approaches 1, the CPE approaches the behavior of an ideal capacitor. The relation between these two terms can be expressed as follows [30]:

$$C_{dl} = Y_0(Y_0 R_{Ct})^{(1-n)/n} \tag{4}$$

The CPE element describes a non-ideal capacitor of non-zero real and imaginary parts. In the Nyquist plot, the high frequency impedance shows inductive behavior. Also, the high frequency part intersects the real axis at a certain distance from the origin. The high frequency part of the impedance spectra is associated with wiring and measurement equipment [31], including the collector plates and metallic parts [21]. The second phenomenon, the intersection distance of the high frequency part is due to the ohmic resistance of the cell. Considering the resistance for electron transport is negligible, this resistance, R_e can be assigned to the proton transport in the electrolyte, i.e. the membrane. This resistance, like the high frequency impedance, resides in series with the rest of the circuit. It is worthwhile to mention that R_e is an important parameter obtained with EIS and used to optimize fuel cell operating conditions. The value of R_e can also be used to correct iR drop in the polarization curve [13]. Impedance data fitting software ZSimpWin 3.20 (EChem Software) was used for fitting the experimental data to the equivalent circuit.

The expression for the Faradaic branch of the circuit was first derived analytically for a general case multi-step single adsorbed intermediate reaction by Armstrong and co-workers [32,33]. Consequently, Harrington and Conway used similar treatment for describing a specific case: impedance of the hydrogen evolution reaction. Melnick and Palmore [14] and Otomo et al. [10] used the same analogy for deriving equivalent circuit for describing methanol electrooxidation on Pt considering single adsorbed intermediate. Considering the complexity of methanol electrooxidation reaction, it is likely that more than one adsorbed intermediate is present. However, our attempt to fit the impedance data with a circuit for two adsorbed intermediates [34] did not result better fits than using circuit in Fig. 8a. It is plausible that only one adsorbed intermediate has significant stability to be detected by EIS, but the consideration of single adsorbed intermediate does not exclude the possibility of other parallel pathway(s) or multiple product formation.

The admittance of the Faradaic branch of the circuit (Fig. 8a) can be expressed by:

$$Y_f = \left(R_{Ct} + \left(j\omega C_P + \frac{1}{R_P} \right)^{-1} \right)^{-1} \tag{5}$$

A particular spectrum could be fitted with more than one possible circuit. The problem of identifying the most probable circuit can be addressed by fitting a range of spectra measured at different, but closely related operating conditions [35]. When the frequency approaches zero (direct current condition), the admittance can be expressed as:

$$Y_f(\omega \to 0) = \frac{1}{R_{dc}} = (R_{Ct} + R_P)^{-1} \tag{6}$$

Here, R_{dc} is the dc resistance and ideally,

$$\frac{1}{R_{dc}} = \frac{\partial I_F}{\partial E} \tag{7}$$

where i_F is the steady-state Faradaic current. Eqs. (6) and (7) present the opportunity of checking the reliability of fitted parameters by allowing comparison between the values of R_{dc}^{-1} obtained from two completely independent sources. Fig. 9 shows the R_{dc}^{-1} values obtained from impedance fitting and polarization measurement at 28 °C for 1.0 M methanol. The Faradaic current density was obtained by subtracting the double layer response from the total polarization current density by using the following formula:

$$I_F = I - C_{dl}\nu \tag{8}$$

where ν is the scan rate. In Fig. 9, although the two sets of values do not exactly overlap, they closely match one another.

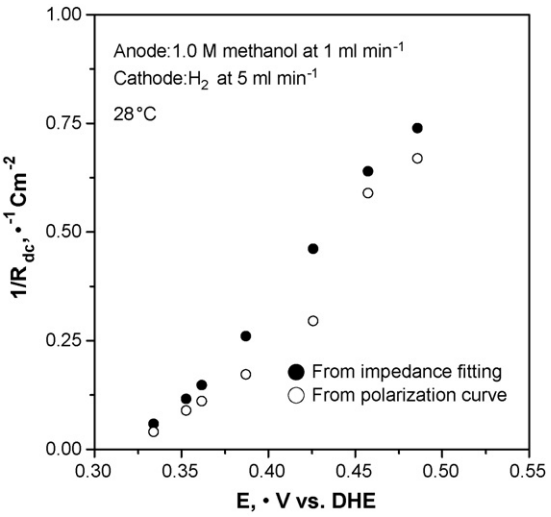

Fig. 9. Comparison between the vales of R_{dc}^{-1} obtained from impedance fitting and polarization measurement at 28 °C. I_F was obtained by: $I_F = I - C_{dl}\nu$ where ν is the scan rate. Scan rate for polarization: 10 mV s^{-1}; anode flow: 1 ml min^{-1}; cathode flow: H_2 at 5 ml min^{-1}. Overpotentials are corrected for iR losses in the cell.

5. Discussion

5.1. Origin of the low frequency inductive loop

The low frequency inductive loop for methanol electrooxidation on Pt and PtRu has been observed by several groups [8–10,13,14]. Similar behavior has also been observed for the electrooxidation of H_2/CO [31,36,37]. The inductive loop is usually modeled by using a pseudoinductance in series with a resistance or a pseudocapacitance in parallel with a resistance. In the later case, a negative pseudocapacitance and negative resistance represents the inductive loop. The pseudocapacitance (C_P) is related to steady-state pseudocapacitance (C_ϕ) and for special cases like H_{UPD}, these two quantities become equal [27]. By definition, C_ϕ is as follows [27,28]:

$$C_\phi = q_i \left(\frac{d\theta_{ss}}{dE} \right) \quad (9)$$

where q_i and θ_{ss} are the charge density for monolayer coverage and the steady-state coverage, respectively. Although a negative capacitance makes no physical sense in electrical terms, from the above equation, a negative capacitance can be understood by a decrease in coverage with potential, i.e. a negative slope of coverage versus potential plot. Nevertheless, a negative value of the slope of the isotherm does not always give rise to the inductive behavior, as the interference of the double layer capacitance may mask the inductive behavior [38,39].

Contrary to negative C_P, it is not possible to give a direct physical significance to a negative value of R_P, which one obtains while fitting inductive loops by using circuit shown in Fig. 8a other than the requirement for a positive time constant ($\tau = C_P R_P$). Harrington and Conway suggested that the fitting of an inductive circuit (Fig. 8b) that is mathematically equivalent to the circuit shown in Fig. 8a makes it easier to give mechanistic significance of the elements [27]. In an inductor (L_s) an electromagnetic force (emf) is induced to oppose the current change occurring. This corresponds to the coverage relaxation part of the Faradaic process opposing the coverage-independent charge transfer part (R_{Ct} arm). The role of R_0 is to adjust the phase delay of the current to the value required by the reaction kinetics, instead of the 90° provided by the inductor.

5.2. Kinetics

5.2.1. Below the onset potential

As shown in Fig. 3, the oxidation of methanol on PtRu at room temperature is associated with quite high onset potential of around ~0.31 V. In case of Pt, the potential range from open circuit to ~0.35 V belongs to the hydrogen ionization for the anodic sweep (hydrogen deposition during cathodic sweep). However, this potential region is more complicated for PtRu compared to Pt because of the added reaction steps like ionization of hydrogen on Ru, reoxidation of evolved hydrogen on both Pt and Ru [40], oxidation of Ru (possibly above 0.2 V [41]). In presence of methanol, adsorption and dehydrogenation of methanol and possibly oxidation of methanolic residues may occur. However, we only could detect two distinguishable time constants in the region from the fitting of our data. Considering that one of the time constants (the smaller of the two) is attributed to the relaxation of double layer, it could be concluded that there is only one process that could be detected by our experiment or all the time constants for all the processes are convoluted in the two time constants. A continuous decrease in the values of R_{Ct}^{-1} and C_P have been observed in the potential range tested (0.11 V to before onset) (Fig. 10). Melnick and Palmore also reported a continuous decrease in R_{Ct}^{-1} with increase in potential for methanol oxidation on polycrystalline Pt in the H_{UPD} region [14]. They attributed this phenomenon to increasing coverage of methanol residues as the potential increases. Methanol adsorption on Pt is known to increase with potential [26,42,43]. Therefore, if there is no or slower removal of residues compared to formation, one can expect the R_{Ct}^{-1} to decrease with potential. Both R_{Ct}^{-1} and C_P at a certain potential decrease as the bulk methanol concentration is increased (Fig. 10). The methanol residue stripping experiments (Fig. 5) showed that the coverage of residues increase with the methanol concentration. A lower value of C_P (considering Eq. (9) and the possible relation between C_P and C_ϕ) could mean that the rate of coverage change with the increase in potential decreases as the concentration is increased. Conway and co-workers have observed a decrease in the value of C_P for S poisoned Pd electrode compared to clean Pd for the reaction of hydrogen sorption into Pd [28]. Based on these arguments, we can conclude that there is a build up of surface bound residues before the onset potential.

5.2.2. After the onset potential

After the onset potential, E_{on}, the methanol oxidation current starts increasing with potential (Fig. 3), and inductive behavior in the Nyquist plot appears (Fig. 1). At or close to E_{on}, the value of C_P becomes negative (Fig. 11a). The value of R_P also becomes negative (not shown) to represent the inductive loop. These phenomena indicate a certain change in reaction mecha-

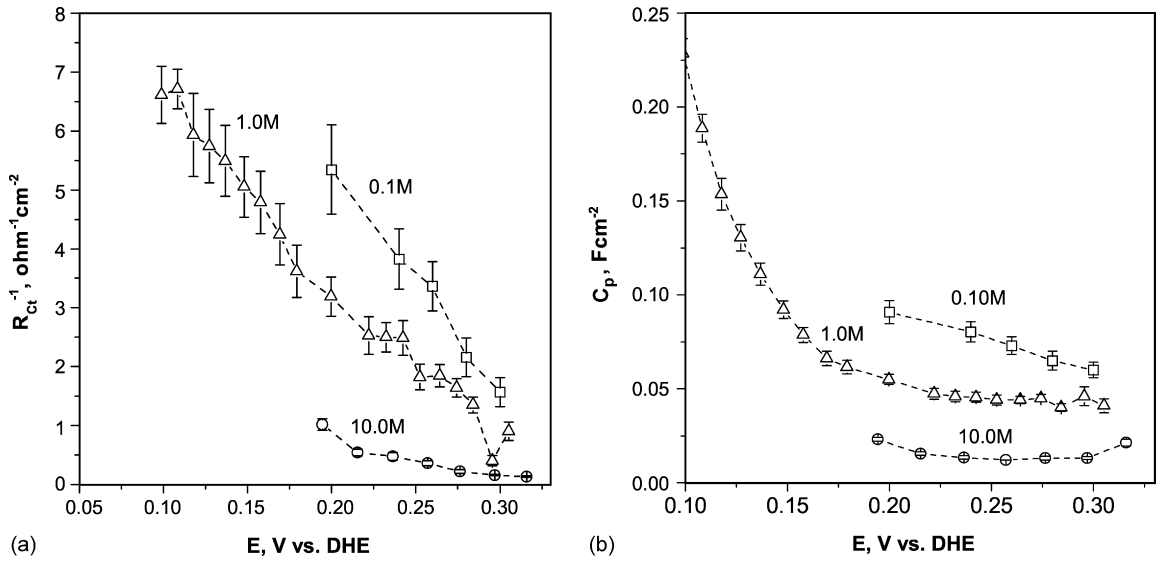

Fig. 10. Dependence of R_{Ct}^{-1} (a) and C_P (b) on potentials for different methanol concentrations below the onset potential at 28 °C. Points: obtained by fitting the impedance data with circuit in Fig. 8a; lines are to guide the eye and not from curve fitting. Bias potentials are corrected for iR losses in the cell.

nism before and after E_{on}. As a negative C_P may be related to decrease of coverage with potential, the beginning of the inductive loop can be the potential where removal of residues starts to make free sites available for further methanol adsorption. However, the advent of the inductive loop is also accompanied by the highest value of R_{Ct} (Fig. 11b) for the potential range examined. The value of R_{Ct} jumps to 135 Ω cm^2 at the onset compared to 1 Ω cm^2 just before E_{on}. The big difference in the value of R_{Ct} with very small change in potential indicates that the R_{Ct} before and after the onset is not related to the same process. In other words, the mechanism of current response is different before and after E_{on}. The gradual decrease of R_{Ct} with potential after E_{on} is an indication that the residue coverage with potential is a bell shaped curve as observed for adsorption/oxidation of methanol by Bagotzky and Vassilev [42] on Pt and Stimming and co-workers on PtRu/C [26]: the coverage of residue is the highest at E_{on} and then it decreases gradually with potential. It is interesting to observe that the inductive loop starts around the same potential (∼0.32 V) for all the concentrations we tested. The conclusion is that the advent of the inductive loop, i.e. the onset of the residue oxidation does not depend on the coverage of the residues. This is also seen in case of residue oxidation during the stripping experiment (Fig. 5). So, it can be concluded that at E_{on}, another reaction step is required to trigger the onset. The reaction is widely speculated and recently shown by Watanabe and co-workers [3,44] as the discharge of water. However, we could not distinguish any reaction which could be related only to the water activation step. The vale of E_{on} moves to more negative potentials with the increase in temperature (Fig. 4). It has been reported in literature that charge for OH adsorption in the double layer region as well as for oxide formation is increased with the increase in temperature only for Pt and not for PtRu [45].

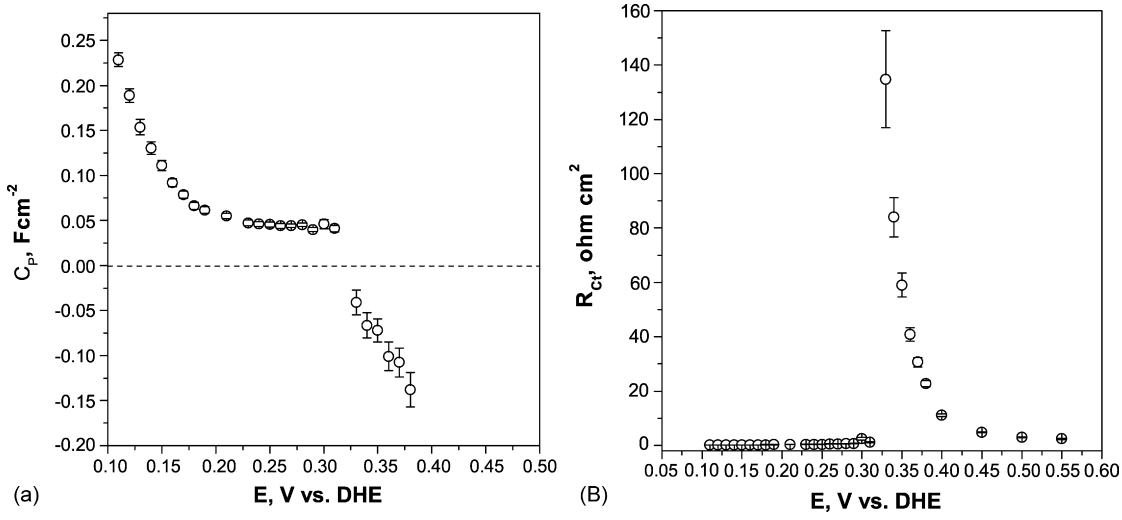

Fig. 11. Dependence of C_P (a) and R_{Ct} (b) on potentials for a wide rage of potential for 1.0 M methanol solution at 28 °C. Notice the changes in R_{Ct} and C_P at ∼0.32 V. This potential is also the onset potential for methanol oxidation.

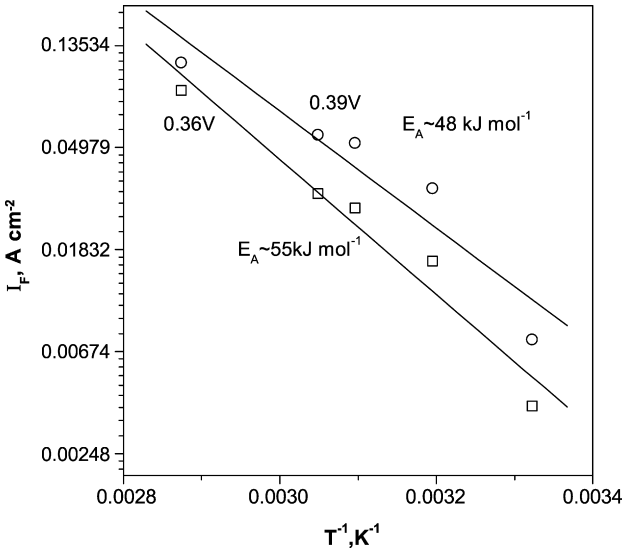

Fig. 12. Plot of $\ln(I_F)$ vs. $1/T$ for calculating the apparent activation energy of methanol oxidation reaction. Points: experimental data; lines: linear fit. Scan rate for polarization: 10 mV s^{-1}; anode flow: 1 ml min^{-1}; cathode flow: H_2 at 5 ml min^{-1}. I_F was obtained by: $I_F = I - C_{dl}\nu$ where ν is the scan rate. Overpotentials are corrected for iR losses in the cell.

Therefore, unlike on Pt [18,46], negative shift of E_{on} on PtRu cannot possibly be attributed mainly to an increased coverage of active surface oxidic species. Besides the fact that methanol adsorption rate increases with temperature, at higher temperatures, Ru sites, along side Pt are also available for adsorption and dehydrogenation of methanol [46]. These lead to higher coverage of surface adsorbed species, possibly CO_{ads} and greater repulsion between the CO_{ads}. As a result, the adsorption energy decreases resulting in weakly adsorbed and more reactive CO_{ads} [47]. Therefore, it is more plausible to attribute the negative shift of E_{on} on PtRu with the increase in temperature mostly to the lowered adsorption energy of the adsorbed residues. The apparent activation energies obtained from plotting $\ln(I_F)$ versus $1/T$ (Fig. 12) are 55 ± 6.7 kJ mol^{-1} and 48 ± 9 kJ mol^{-1} for 0.36 V and 0.39 V, respectively. It is worthwhile to mention that I_F is used for obtaining the activation energy instead of the current density, I, because when I is determined from CV, it contains a contribution from the double layer current. Using I_F gives one the opportunity to observe the effect of temperature or potential on only the methanol oxidation reaction. The decrease in activation energy with increase potential indicates that the effect of temperature on the reaction is lowered as the potential is increased possibly due to the saturation effect. In other words, both temperature and potential push the reaction in the same direction. The Tafel slope (b) obtained from both $\log(R_{Ct}^{-1})$ versus E and $\log(I_F)$ versus E (Fig. 13) at 28 °C, 50 °C and 75 °C are around 100 mV decade^{-1}, indicating that the reaction mechanism possibly remains unchanged throughout the temperature range tested here.

5.3. Comparison of performances of different MEAs

The same equivalent circuit shown in Fig. 8a has been used for fitting the spectra shown in Fig. 7 except the spectrum of

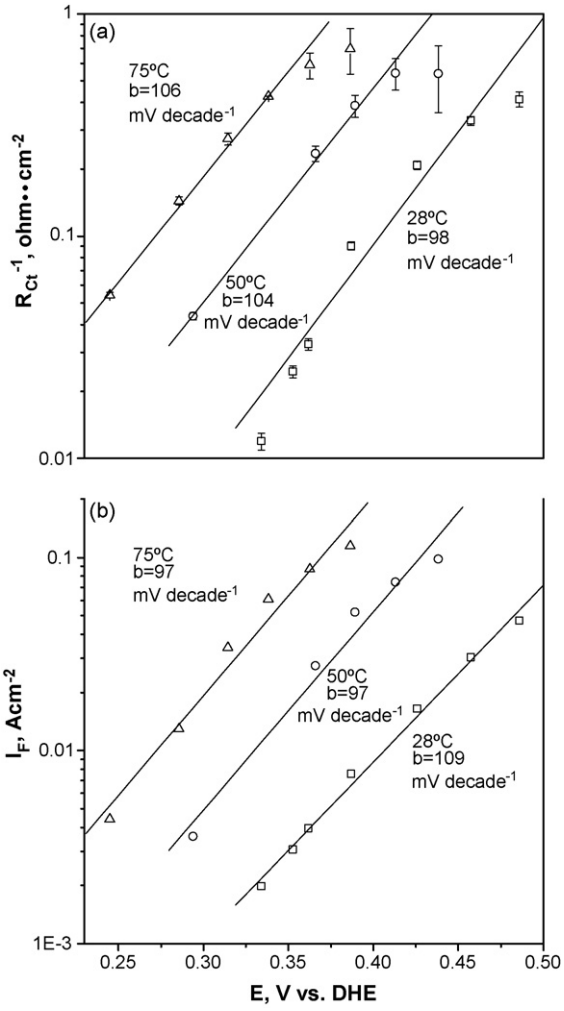

Fig. 13. Plot of $\log(R_{Ct}^{-1})$ vs. E (a) and $\log(I_F)$ vs. E (b) for obtaining the Tafel slope. Points: experimental data; lines: linear fit. Scan rate for polarization: 10 mV s^{-1}; anode flow: 1 ml min^{-1}; cathode flow: H_2 at 5 ml min^{-1}. I_F was obtained by: $I_F = I - C_{dl}\nu$ where ν is the scan rate. Overpotentials are corrected for iR losses in the cell.

the JM MEA. To fit the spectrum, an extra component, a parallel combination of a capacitor (0.0093 ± 0.002 F cm^{-2}) and a resistor ($0.112 \pm 0.01\ \Omega$ cm^2) in series with the circuit shown in Fig. 8a has been used. The very small time constant of the added component suggests that it is possibly a contribution from the cathode/reference electrode. Table 2 shows the extracted parameters from the fitted circuits for the spectra shown. The IRD and JM MEAs have lower membrane resistance ($\sim 1\ \Omega$ cm^2) compared to the Flame MEA ($\sim 1.3\ \Omega$ cm^2). Interestingly, a thinner membrane, Nafion 112 was used for the Flame MEA. The thinner membrane may not have fared as well as the thicker membrane upon exposure to the temperature and pressure applied during MEA preparation (discussed in more detail in the next section).

The charge transfer resistances follow the order Flame ($\sim 11\ \Omega$ cm^2) > JM ($7\ \Omega$ cm^2) > IRD ($4\ \Omega$ cm^2) and the current densities follow the order IRD > JM > Flame. Therefore, R_{Ct} is certainly a parameter that is related to the difference in performance; the trend is that the higher the value of R_{Ct}, the lower the

Table 2
Extracted parameters of the spectra shown in Fig. 7

MEA	Bias potential (V)	L (H cm^2)	R_e (Ω cm^2)	Y_0 (S-s^n cm^{-2})	n	C_{dl} (F cm^{-2})	R_{Ct} (Ω cm^2)	C_P (F cm^{-2})	R_P (Ω cm^2)	X^2
IRD	0.4	$1.22 \times 10^{-6} \pm 3.4 \times 10^{-8}$	1.15 ± 0.004	0.216 ± 0.009	0.85 ± 0.18	0.213	4.245 ± 0.34	-0.162 ± 0.033	-3.262 ± 0.33	9.9×10^{-4}
JM	0.4	$2.4 \times 10^{-6} \pm 3.4 \times 10^{-8}$	1.0 ± 0.006	0.098 ± 0.005	0.7957 ± 0.02	0.09	6.846 ± 0.62	-0.06 ± 0.01	-5.231 ± 0.6	8.75×10^{-4}
Flame	0.4	$1.15 \times 10^{6} \pm 1.58 \times 10^{-7}$	1.363 ± 0.02	0.052 ± 0.01	0.77 ± 0.05	0.044	11.33 ± 2.82	-0.058 ± 0.04	-7.649 ± 2.76	6.4×10^{-3}

value of current density. The value of R_{Ct} decreases because of the increase in the three-phase region [48,49], improved transport properties in the catalyst layer [49], and obviously, due to better inherent catalytic activities of the material.

Electrochemically active surface areas may be estimated by the values of C_{dl} which is usually proportional to the active surface area [50–55]. In fact, Conway and co-workers have suggested the use of C_{dl} in determining relative electrochemically active surface area as 'quite reliable' [54]. This method is especially useful for unsupported catalyst [55]. However, caution should be exercised while estimating electroactive area from C_{dl}. The value of C_{dl}, besides surface roughness, depends also on the type of active materials, applied potential and conductivity of the electrolyte [56,57]. Moreover, C_{dl} also changes a great deal when surface oxide is formed compared to metallic surfaces [29,58]. In spite of the above limitations, this method could be very useful for comparing the electroactive surface areas of different electrodes with same active elements if applied with caution. Application of this method is more attractive on electrodes which have active catalysts like PtRu because unlike Pt, it is not possible to accurately estimate the electroactive area of PtRu from the charge of the H_{UPD} region. The overlap of currents from hydrogen ionization from Pt, hydrogen ionization from Ru and possible oxidation of Ru (during forward sweep) makes this process very unreliable [40,59]. Furthermore, the H_{UPD} and the double layer region overlap in case of PtRu and this causes a real problem in terms of selecting the region in the CV for integration to estimate the charge. CO stripping method is also not accurate enough because of the uncertainty of CO adsorption stoichiometry on both Pt and Ru [59]. More complicated methods like underpotential deposition of Cu and a combination of $(COOH)_2$ oxidation and CO stripping have been proposed for accurate estimation of electroactive surface area for PtRu [59,60]. The underlying assumptions for using the C_{dl} method for the purpose of this article are that the PtRu in all the three anodes are same material and that the electrolyte conductivity in the catalyst layer does not vary significantly between the anodes. The values of the double layer capacitances calculated by using the value of Y_0 and n are shown in Table 3. The IRD anode has the highest value of C_{dl} of $\sim$0.2 F cm^{-2} (Table 3), indicating that it has the highest electrochemically active surface area of the MEAs tested. This result is not surprising because the IRD anode not only has higher metal loading (Table 1) but also highly optimized as it is a state of the art product. It can be seen from Table 3 that the ratios of the values of C_{dl} between two different MEAs at 0.4 V are very close to the ratios of the current densities. The values of $C_{dl}/(C_{dl})_{IRD}$ and $i/(i)_{IRD}$ are shown as examples in

Table 3
Current density and double layer capacitance for different MEAs

Potential	MEA	Current density (i) (mA cm^{-2})	C_{dl} (F cm^{-2})	i/i_{IRD}	$C_{dl}/(C_{dl})_{IRD}$
0.4 V	IRD	$\sim$78	0.213	1	1
	JM	$\sim$37	0.09	0.47	0.42
	Flame	$\sim$17	0.044	0.22	0.22

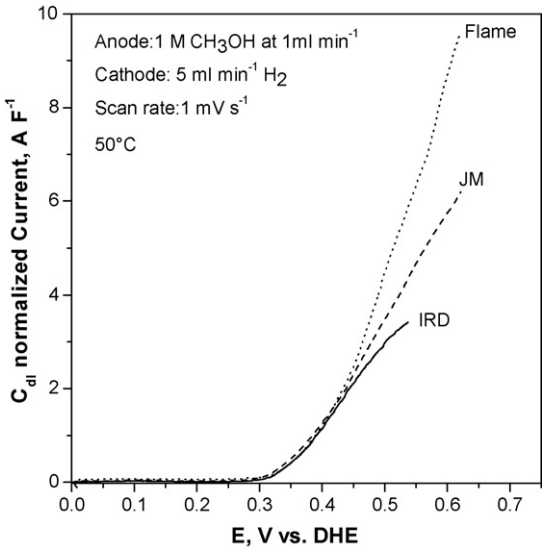

Fig. 14. Double layer normalized currents for three different MEAs at 50 °C. Scan rate: 1 mV s^{-1}; anode flow: 1 ml min^{-1}; cathode flow: H_2 at 5 ml min^{-1}. Overpotentials are corrected for iR losses in the cell.

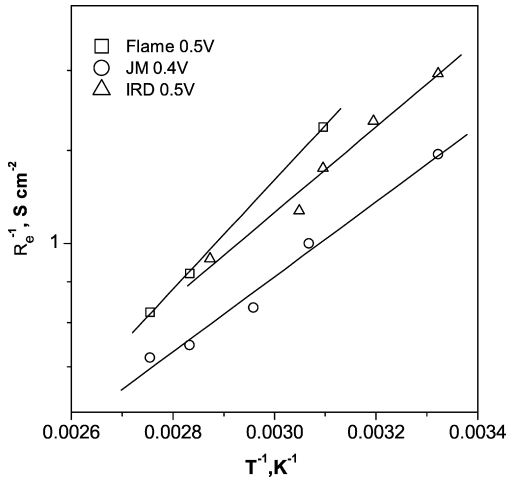

Fig. 15. Plot of $\ln(1/R_e)$ vs. $1/T$ for calculating the average conductivity of the membranes in different MEAs. The equation resulted from the linear fittings are: $\ln(1/R_e) = -2.14 + 731.35/T$, $R = 0.99$ for IRD; $\ln(1/R_e) = -1.98 + 640/T$, $R = 0.99$ for JM; $\ln(1/R_e) = -2.7 + 932.85/T$; $R = 0.997$ for Flame.

Table 3. To compare the intrinsic activity of the active sites, the polarization current was normalized in terms of the double layer capacitance obtained at 0.4 V. It is very interesting to observe that the C_{dl} normalized activities of all the three catalysts are very similar from 0.3 V to 0.45 V (Fig. 14). Moreover, 0.4 V is too low a potential for the activity to be affected by mass transfer limitations. Therefore, the difference between the performances of the three anodes tested here are mainly due to the difference in the electrochemically active areas. It can be seen from Fig. 14 that after ~0.45 V, the activities deviate from one catalyst to the other with the Flame catalyst showing the highest intrinsic activity and IRD the lowest. However, one should keep in mind that the deviations could also be due to normalization of the current with the values of C_{dl} estimated at 0.4 V for the whole potential range. Ideally, one should normalize the current at each potential with the C_{dl} estimated at that potential.

5.4. Membrane conductivity

The activation energy for proton transport in the membrane was determined by using an Arrhenius type relationship

$$\frac{1}{R_e} = A \exp\left(\frac{E_A}{RT}\right) \tag{10}$$

where A is the pre-exponential factor, E_A the activation energy and T is the absolute temperature. The specific conductivity is given by the following relation:

$$\sigma = \frac{d}{R_e} \tag{11}$$

where σ is the specific conductivity (S cm^{-1}) and d is the thickness of the membrane. A plot of $\ln(1/R_e)$ versus $1/T$ gives the activation energy of proton transport (Fig. 15). The specific conductivity at a given temperature can be calculated by using Eqs. (10) and (11). The estimated specific conductivity for membranes of the MEAs at 50 °C is shown in Table 4. The membranes in the MEAs prepared with Nafion 117 (IRD and JM) have higher specific conductivity (~0.02 S cm^{-1}) compared to the membrane in the Flame MEA prepared with Nafion 112 (~0.005 S cm^{-1}). The estimated conductivity values reported in the literature for Nafion 117 is 0.07–0.14 S cm^{-1} and for Nafion 112 is 0.1–0.144 S cm^{-1}, depending on the temperature and electrolyte [61]. The general conclusion is that our experimentally determined Nafion specific conductivities are less than expected for both Nafion 117 and Nafion 112. The low specific conductivity is much more pronounced for Nafion 112; ~1/25 times of that found in the literature. This could be attributed to the deterioration of the membrane by the pressure and temperature applied during the MEA preparation and/or poor contact of the reaction zone with the membrane. It has been reported that thermal treatment can irreversibly change the properties of Nafion 117 membrane [62]. Cappadonia et al. observed that Nafion 117 membrane hot pressed at 130 °C for 2 min remained 'dry' even after 72 h of storage in water or water vapor [63]. Freire et al. related the changes in the Nafion membrane to the collapse of the hydrophilic cluster consisted of sulphonic groups in Nafion upon heating. This renders the membrane hydrophobic making it difficult to hydrate again [22]. The thinner membrane (Nafion 112) is more likely to be affected by the MEA fabrication procedure than the thicker membrane (Nafion 117), giving rise to much lower specific conductivity while inside an MEA than the real specific conductivity. However, the poor contact between

Table 4
Specific conductivities of membranes in the MEAs

MEA	Membrane	Thickness (μm[a])	Specific conductivity (S cm^{-1})
Flame	Nafion 112	60	~0.005
JM	Nafion 117	200	~0.02
IRD	Nafion 117	200	~0.018

[a] Taken from Ref. [61].

the membrane and the reaction zone could also contribute to the lower than expected conductivity of the membranes. Therefore, the specific conductivity values reported here should be considered as the property of the MEAs rather than the membranes. This method of estimating conductivity can be used in selecting optimum temperature and pressure for hot pressing.

6. Conclusions

Only single adsorbed intermediate of methanol oxidation on nanoparticulate PtRu have been detected by EIS. The onset potentials are coincident with the appearance of the inductive impedance. Before the onset, the observed gradual increase in the charge transfer resistance with potential has been attributed to the blocking of active sites with methanol residues. The gradual decrease in the value of charge transfer resistance with increase in potential after the onset indicates a decrease in residue coverage and more available sites for the reaction to proceed. The appearance of the inductive loop (i.e. the onset potential) does not depend on the methanol concentration (i.e. the residue coverage).

The application of EIS in performance analysis has been demonstrated by investigating the methanol oxidation performance of three different MEAs. The applicability of the double layer capacitance as a plausible method for comparing the electroactive areas between different electrodes has been discussed. Double layer capacitance has been used to obtain the intrinsic activities of the PtRu anodes in three electrodes. For the three MEAs we have tested, differences in performance originate mainly from the available three-phase region and not from the intrinsic activity of the catalysts. Further, it has been shown that the membranes in the MEAs tested in this work have much lower proton conductivities compared to literature reported specific conductivity values, because of membrane deterioration during hot pressing and/or poor contact of the membrane with the reaction zone.

Acknowledgements

This work was supported by PSO (project 5357). Center for Individual Nanoparticle Functionality (CINF) is sponsored by The Danish National Research Foundation. The authors wish to thank IRD Fuel Cells A/S for the collaboration. Assistance form SGL Carbon is also gratefully acknowledged.

References

[1] B.D. McNicol, D.A.J. Rand, K.R. Williams, J. Power Sources 83 (1999) 15–31.
[2] M.P. Hogarth, T.R. Ralph, Platinum Met. Rev. 46 (2002) 146–164.
[3] T. Yajima, H. Uchida, M. Watanabe, J. Phys. Chem. B 108 (2004) 2654–2659.
[4] G.T. Burstein, C.J. Barnett, A.R. Kucernak, K.R. Williams, Catal. Today 38 (1997) 425–437.
[5] R. Jiang, H.R. Kunz, J.M. Fenton, J. Electrochem. Soc. 152 (2005) A1329–A1340.
[6] I.D. Raistrick, J.R. Macdonald, D.R. Franceschetti, Impedance Spectroscopy, Emphasizing Solid Materials and Systems, John Wiley & Sons, New York, 1987, pp. 39–40.
[7] J.T. Müller, P.M. Urban, J. Power Sources 75 (1998) 139–143.
[8] J.T. Müller, P.M. Urban, W.F. Holderich, J. Power Sources 84 (1999) 157–160.
[9] I.-M. Hsing, X. Wang, Y.-J. Leng, J. Electrochem. Soc. 149 (2002) A615–A621.
[10] J. Otomo, X. Li, T. Kobayashi, C.-J. Wen, H. Nagamoto, H. Takahashi, J. Electroanal. Chem. 573 (2004) 99–109.
[11] H. Fukunaga, T. Ishida, N. Teranishi, C. Arai, K. Yamada, Electrochim. Acta 49 (2004) 2123–2129.
[12] W. Sugimoto, K. Aoyama, T. Kawaguchi, Y. Murakami, Y. Takasu, J. Electroanal. Chem. 576 (2005) 215–221.
[13] D. Chakraborty, H. Bischoff, I. Chorkendorff, T. Johannessen, J. Electrochem. Soc. 152 (2005) A2357–A2363.
[14] R.E. Melnick, G.T. Palmore, J. Phys. Chem. B 105 (2001) 1012–1025.
[15] R.E. Melnick, G.T. Palmore, J. Phys. Chem. B 105 (2001) 9449–9457.
[16] J.-P. Diard, N. Glandut, P. Landaud, B.L. Gorrec, C. Montella, Electrochim. Acta 48 (2003) 555–562.
[17] S. Sanicharane, A. Bo, B. Sompalli, B. Gurau, E.S. Smotkin, J. Electrochem. Soc. 5 (2002) A554–A557.
[18] J. Jiang, A. Kucernak, J. Electroanal. Chem. 576 (2005) 223–236.
[19] L. Liu, R. Viswanathan, R. Liu, E.S. Smotkin, Electrochem. Solid State 1 (1998) 123–125.
[20] A. Havranek, K. Wippermann, J. Electroanal. Chem. 567 (2004) 305–315.
[21] A.G. Hombrados, L. Gonzĭalez, M.A. Rubio, W. Agila, E. Villanueva, D. Guinea, E. Chinarro, B. Moreno, J.R. Jurado, J. Power Sources 151 (2005) 25–31.
[22] T.J.P. Freire, E.R. Gonzalez, J. Electroanal. Chem. 503 (2001) 57–68.
[23] J.S. Lee, K.I. Han, S.O. Park, H.N. Kim, H. Kim, Electrochim. Acta 50 (2004) 807–810.
[24] H.N. Dinh, X. Ren, F.H. Garzon, P. Zelenay, S. Gottesfeld, J. Electroanal. Chem. 491 (2000) 222–233.
[25] J.T. Müller, P.M. Urban, J. Power Sources 75 (1998) 139–143.
[26] T. Seiler, E.R. Savinova, K.A. Friedrich, U. Stimming, Electrochim. Acta 49 (2004) 3927–3936.
[27] D.A. Harrington, B.E. Conway, Electrochim. Acta 32 (1987) 1703–1712.
[28] S.Y. Qian, B.E. Conway, G. Jerkiewicz, Int. J. Hydrogen Energy 25 (2000) 539–550.
[29] P.S. Germain, W.G. Pell, B.E. Conway, Electrochim. Acta 49 (2004) 1775–1788.
[30] ZSimpWin Technical Notes, http://www.echemsw.com/note24.htm.
[31] J.-M. Hu, J.-Q. Zhang, C.-N. Cao, I.-M. Hsing, Electrochim. Acta 49 (2004) 5227–5234.
[32] R.D. Armstrong, M. Henderson, J. Electroanal. Chem. 39 (1972) 81–90.
[33] R.D. Armstrong, K. Edmondson, Electrochim. Acta 18 (1973) 937–943.
[34] G.Ø. Lauvstad, R. Tunold, S. Sunde, J. Electrochem. Soc. 12 (2002) E497–E505.
[35] M.V. ten Kortenaar, C. Tessont, Z.I. Kolar, H. van der Weijde, J. Electrochem. Soc. 146 (1999) 2146–2155.
[36] M. Ciureanu, H. Wang, Z. Qi, J. Phys. Chem. B 103 (1999) 9645–9657.
[37] N. Wagner, M. Schulze, Electrochim. Acta 48 (2003) 3899–3907.
[38] L. Bai, B.E. Conway, J. Electrochem. Soc. 138 (1991) 2897–2907.
[39] J.-P. Diard, B. Le Gorrec, C. Montella, J. Electroanal. Chem. 326 (1992) 13–36.
[40] S. HadzI-Jordanov, H. Angerstein-Korlowska, M. Vukovlc, B.E. Conway, J. Phys. Chem. 81 (1977) 2271–2279.
[41] H.A. Gasteiger, N. Marković, P.N. Ross Jr., E.J. Cairns, J. Phys. Chem. B 97 (1993) 12020–12029.
[42] V.S. Bagotzky, Y.B. Vassilev, Electrochim. Acta 12 (1967) 1323–1343.
[43] Z. Jusys, R.J. Behm, J. Phys. Chem. B 105 (2001) 10874–10883.
[44] T. Yajima, N. Wakabayashi, H. Uchida, M. Watanabe, Chem. Commun. (2003) 828–829.
[45] A.V. Tripkovic, S. Štrbac, K.Dj. Popovic, Electrochem. Commun. 5 (2003) 484–490.
[46] H.A. Gasteiger, N. Marković, P.N. Ross Jr., E.J. Cairns, J. Electrochem. Soc. 141 (1994) 1795–1803.
[47] N. Marković, P.N. Ross Jr., Surf. Sci. Rep. 45 (2002) 118–229.
[48] J.H. Kim, H.Y. Ha, I.H. Oh, S.A. Hong, H.N. Kim, H.I. Lee, Electrochim. Acta 50 (2004) 797–802.

[49] T.E. Springer, T.A. Zawodzinski, M.S. Wilson, S. Gottesfeld, J. Electrochem. Soc. 143 (1996) 587–599.
[50] G. Wu, Y.-S. Chen, B.-Q. Xu, Electrochem. Commun. (2005) 1237–1243.
[51] J.H. Kim, H.I. Lee, S.A. Hong, H.Y. Ha, J. Electrochem. Soc. 153 (2005) A2345–A2351.
[52] M. Mastragostino, A. Missiroli, F. Soavi, J. Electrochem. Soc. 151 (2004) A1919–A1924.
[53] Z. Siroma, T. Sasakura, K. Yasuda, M. Azuma, Y. Miyazaki, J. Electroanal. Chem. 546 (2003) 73–78.
[54] R. Šimpraga, G. Tremiliosi-Filho, S.Y. Qian, B.E. Conway, J. Electroanal. Chem. 424 (1997) 141–151.
[55] S. Wasmus, A. Küver, J. Electroanal. Chem. 461 (1999) 14–31.
[56] L. Bai, L. Gao, B.E. Conway, J. Chem. Soc., Faraday Trans. 89 (1993) 243–249.
[57] S. Trasatti, O.A. Petrii, Pure Appl. Chem. 63 (1991) 711–734.
[58] W.G. Pell, A. Zolfaghari, B.E. Conway, J. Electroanal. Chem. 532 (2002) 13–23.
[59] C.L. Green, A. Kucernak, J. Phys. Chem. B 106 (2002) 1036–1047.
[60] C. Bock, B. MacDougall, J. Electrochem. Soc. 150 (2003) E377–E383.
[61] S. Slade, S.A. Campbell, T.R. Ralph, F.C. Walsh, J. Electrochem. Soc. 149 (2002) A1556–A1564.
[62] T.A. Zawodzinski, C. Derouin, S. Radzinski, R.J. Sherman, V.T. Smith, T.E. Springer, S. Gottesfeld, J. Electrochem. Soc. 140 (1993) 1041–1047.
[63] M. Cappadonia, J.W. Erning, S.M.S. Niaki, U. Stimming, Solid State Ionics 77 (1995) 65–69.